ISSN: 2447-3359

REVISTA DE GEOCIÊNCIAS DO NORDESTE

Northeast Geosciences Journal

v. 9, nº 2 (2023)

https://doi.org/10.21680/244-3359.2023v9n2ID32658

3D Shape Features for Objects Classification from Terrestrial Lidar Point Clouds

Descritores de Forma 3D para Classificação de Objetos em Nuvens de Pontos Lidar Terrestre

Jorge Antonio Silva Centeno[1]; Elizabete Bugalski de Andrade Peixoto[2]

[1] Federal University of Paraná/ Department of Geomatics, Curitiba/PR, Brasil. Email:centeno@ufpr.br
ORCID: https://orcid.org/0000-0002-2669-7147

[2] Lactec, Environment Sector, Curitiba/PR, Brasil. Email: Elizabete.peixoto@lactec.com.br
ORCID: https://orcid.org/ 0000-0001-7430-8727

Abstract: A mobile laser scanner is a valuable tool to collect 3D information especially in urban regions, where vertical objects, like walls, poles and trees, need to be mapped. The collected point clouds can be used to segment objects and classify them according to their shape. Nevertheless, the segmentation and classification steps still need tools to analyze 3D point clouds. In this paper it is introduces a method to describe 3D shape from point clouds obtained by mobile laser scanner within the context of classification of urban furniture. The initial aim is to describe the 3D shape of objects located at the top of poles, but the approach can be extended to other objects. For this purpose, the distribution of the points is analyzed with help of the eigenvalues of the variance-covariance matrix. It is proposed the use of two parameters, one related to planarity and another to elongation, that are normalized in the range between zero and one, which allows easier description of the shape in terms of just two well-known terms.

Keywords: **S**hape features; Point cloud processing; LiDAR; 3D Modelling.

Resumo: O laser scanner móvel é uma ferramenta valiosa para coletar informações 3D, especialmente em regiões urbanas, onde objetos verticais, como paredes, postes e árvores, precisam ser mapeados. As nuvens de pontos coletadas podem ser usadas para segmentar objetos e classificá-los de acordo com sua forma. No entanto, as etapas de segmentação e classificação ainda precisam de ferramentas para analisar nuvens de pontos 3D. Neste artigo é apresentado um método para descrever a forma 3D a partir de nuvens de pontos obtidas por scanner laser móvel dentro do contexto de classificação de mobiliário urbano. O objetivo inicial é descrever a forma de objetos instalados em postes, mas a abordagem pode ser estendida a outros objetos. Para tanto, a distribuição dos pontos é analisada com o auxílio dos autovalores da matriz variância-covariância e os respectivos autovalores. Propõe-se a utilização de dois parâmetros, um relacionado à planaridade e outro ao alongamento, que são normalizados na faixa entre zero e um, o que permite uma descrição mais fácil da forma em termos de apenas dois termos bem conhecidos.

Palavras-chave: Análise de forma, Processamento de nuvens de pontos; LiDAR; Modelagem 3D

Received: 25/05/2023; Accepted: 14/11/2023; Published: 22/11/2023.

1. Introduction

The surveying scenario experienced the effect of recent developments in terms of mobile systems, such as mobile laser scanner systems capable of collecting a dense 3D point cloud over a large area at the ground level. This development opened new challenges to the scientific community in terms of methods to detect and model 3D objects, especially in urban areas. There are studies concerning modeling of façades, like Faltýnová et al. (2016) or Haghighatgou et al (2022), trees, like Sirmacek, and Lindenbergh (2015) or Suwardhi et al (2022), and poles, like Fukano and Masuda (2015), Shi et al (2018) or Li, and Cheng (2020). Concerning the latter, the task is to map existing poles and distinguish between their uses based upon their shape and mainly upon the shape of the attached objects.

Pole detection methods have similarity with methods aimed at detecting trees, vertical elements of the landscape. Some works, such as Yu et al. (2015) or Li, and Cheng (2020) are examples of point clouds processing for detection of poles with terrestrial LiDAR. In a broader sense, pole detection and classification methods are also included in the more general detection of urban furniture problems and are discussed in works like Fukano and Masuda (2015), Li et al. (2016) or Li et al. (2019).

As the problem is to detect and classify urban furniture, pole detection methods usually begin with the classification of ground points, which enables computing a normalized representation that stores the height of the objects above the ground. The methods of terrain filtering from aerial LiDAR can be applied for this purpose. When dealing with mobile terrestrial scanner data, alternative solutions were proposed to extract the bare soil, as for example in Ibrahim and Lichti (2012), who propose splitting the point cloud into two main segments, ground, and non-ground, by analyzing the local density of the point cloud. It is assumed that points on the ground are in regions of lower density and therefore the number of points inside a sphere of the defined radius is counted. Yan et al (2016) also apply ground filtering based on the statistical distribution of points. A more complex approach is described in Denis et al. (2010), who propose an algorithm based on region growing, taking as seed the point with the minimal height of each scanned line. There are other options to isolate pole-like objects in the literature. For example, Yang and Dong (2013) proposed analyzing the neighborhood of a point searching for planar regions that would be associated to walls and roads and, therefore, can be discarded. In Yu et al. (2015) ground points were segmented dividing the cloud in voxels and the computing their height. Based upon a height threshold the ground could be detected and the objects above the ground separated for posterior classification. To ease pole-like object detection, walls can be removed in advance because they are usually large planar patches located by the roadside.

From this point up, the pole detection techniques vary. Among the best known are the slicing techniques and those based upon the detection of cylinders, as described in Huang and You (2005). Slicing consists in defining a surface parallel to the ground at a height specified by the user. This method, also described in Luo and Wang (2005), assumes that the poles are vertical structures and will intercept this virtual surface. To improve the method, several surfaces are produced at different heights. Assuming that poles are cylinders, Press and Austin (2004) and Díaz-Vilarino et al. (2015) propose to apply the Hough transform to identify the points belonging to a circle. Another way to model the section of the poles would be applying the RANSAC method for detecting circular structures, as described in Bolles and Fischler (1981). A different approach is described in Rodríguez-Cuenca et al (2015). They propose the use of a classification scheme based upon the Mahalanobis distance. First, the point cloud is segmented, and vertical clusters (pillars) are detected using voxels. Then, the Reed and Yu (1990) method (based upon the Mahalanobis distance) is applied to detect pillars that represent a vertical element.

In terms of classification, the focus is the analysis of the pole top, where objects like shields or lamps may be installed. The approach can be very simple, based on height thresholding (Yu et al, 2015) or even include methods of artificial intelligence, as shown in Guan et al (2015). Most of the approaches for extracting pole-like objects are based on shape features because they provide important geometric clues. For example, after the pole-like objects are detected, Fukano and Masuda (2015) propose to divide the point cloud into spatially simpler parts: pole and top object (shield, lamp, box, etc.). When it comes to analyze the object on the top, the point cloud of this region is classified using the following variables: Sizes of the bounding box; Eigenvalues; Ratios of eigenvalues: Numbers of subsets (elements); Distances between elements and the Ratios of edge directions.

Other studies were performed for this purpose and presented in the literature. Some of them are discussed below. A common practice is to use the eigenvalues (λ_1, λ_2, λ_3) computed from the covariance matrix of the 3D coordinates of the point cloud. A summary of the proposed features is listed in tables 1, 2 and 3.

Table 1 – Comparison of features that describe the 3D size of the point cloud.

Feature	Formula	Source
omnivariance	O = □1 □2 □3	Weinmann et al. (2013)
sum of eigenvalues	Su=□1 + □2 + □3	Weinmann et al. (2013)

Source: The authors (2023).

Two features used to describe volume are the sum of the eigenvalues and the omnivariance (Table 1). As the sum of the eigenvalues is equal to the total variance, it is reasonable to use the sum of the eigenvalues as a measure of volume or size. The omnivariance is the geometric mean of the eigenvalues and describes the mean size of the cloud.

Describing shape is more complex and some studies were devoted to proposing shape parameters based on the eigenvalues. One common aspect of such studies is the fact that they were originally proposed to segment 2 ½ point clouds. Therefore, features like curvature and planarity are commonly used. To classify and discuss such features, the main features found in the literature were grouped and are listed in table 2. Although they may receive different names for the same property, we tried to create three categories: One related to elongation, the second related to planarity and the last one the volumetric variation.

Linearity may also be described as elongation and is characterized by the relative larger dispersion in one direction and very small dispersion around this axis. This is described by the relative size of the first eigenvalue, for example in Weinmann et al. (2013), Li et al. (2016), or Fukano and Masuda (2015)). A common practice, noticed in Table 2, is to compare the first and the second eigenvalues.

To describe planar objects, the approaches vary but a common aspect is to measure the contrast between the second and third eigenvalues, like in Weinmann et al. (2013), Li et al. (2016), or Ordoñez et al (2017). On the other hand, Yokohama et al (2011) use the difference between the first and the last eigenvalues.

Features to describe objects that have considerable dimension along the three main axes (3D) are also proposed and basically they use the relative size of the third eigenvalue: Weinmann et al. (2013) propose the sphericity feature; Li et al. (2016) or Ordoñez et al (2017) the volumetry factor. The variation of the curvature of a surface, proposed by Rusu (2009), is based on the relative size of the smallest eigenvalue, and can also be linked to a measure to distinguish planarity and volumetry. This curvature feature is presented as a shape feature in Teo and Chiu (2016). Yokohama et al (2011) prefer to apply the value of the smallest eigenvalue corrected by an adjusted factor.

There are other features listed in the literature and summarized in table 3 that can aid in the classification step. They are related to other properties, such as anisotropy and eigentropy. As Anisotropy describes the fact that the cloud is directionally dependent, it also can be included as a measure of elongation. Eigentropy could be linked to the size.

The comparison reveals some common facts, for example the linearity is measured comparing the first and the second eigenvalues. Planarity is given by the comparison of the second and third eigenvalues. Finally, the dispersion of the cloud in three dimensions is measured by comparing the third and the first eigenvalues.

Recent advances are deep learning models which also introduce solutions to the problem. But in this case the features are extracted by a neural net. Examples can be found in Guan et al (2018) who proposed a classifier based on a supervised Gaussian–Bernoulli deep Boltzmann machine model, or Huang J. and You (2016), who used 3D Convolutional Neural Network. The advantage of deep learning approaches is that they do not require spatial features to be proposed "a priori". In the last decade, deep neural networks made remarkable contributions for image segmentation and classification using the raster structure of images and videos. A comprehensive and up-to-date review of the use of deep learning models to segment and classify point clouds is presented in Fernandes et al (2020). At a first stage, its application to process LiDAR point clouds found difficulties because such point clouds have irregular distribution and are not structured as images. Therefore, it became difficult for the deep learning models to extend the convolution concept for point cloud processing. Some efforts were made to apply the convolution concept to voxels. Hrutka et al. (2022) applied the voxel concept to segment point clouds and stated the advantage of reducing the number of points and therefore processing time. On the other hand, detail is lost in the near range, where the point cloud density is high. Other researchers tried to project the 3D point cloud to a 2D space to apply the 2D convolution, for instance computing images from the point cloud considering different points of view, like Su et al. (2015), or projecting 3D features on a 2D space, like Alonso et al (2020). As Alonso et al. (2020) state, the projection causes accuracy loss of the original data, which results in inaccurate classification, although such methods are faster.

More recent research developed deep learning models that can use 3D sparce data to segment and classify point clouds, like PointNet or PointNet++, proposed by Qi et al. (2017a) and Qi et al. (2017b). PointNet++, a follow-up work of PointNet, groups 3D points into regions and computes local features for each region using the convolutional net PointNet. For this purpose, the point cloud is normalized in terms of orientation and geometric size, and then a series of features is computed for each point according to its position and context within the cloud. Methods that are based on deep learning models use machine computed features, which are not known by the user and therefore difficult to understand. Such parameters are derived from a large set of samples and are highly dependent of the representativity of the samples. On the other hand, human proposed features can also be used to feed neural nets, as shown in Özdemir et al. (2019), which would speed up the process, but reduce its automation aspect. Our work is a contribution within the last alternative and focuses on understanding those spatial features. Therefore. the present study focuses on the discussion of spatial features for classification purposes as they are a common practice in many pole classification studies.

Table 2 – Comparison of 3D shape features

Source	Linearity	Planarity	Volume
Weinman et al. (2013)	$1- \lambda_2 / \lambda_1$	$(\lambda_2 - \lambda_3) / \lambda_1$	λ_3 / λ_1
Li et al.(2016)	$1- (\lambda_2, / \lambda_1)^{1/2}$	$(\lambda_2^{½} - \lambda_3^{½}) / \lambda_1^{½}$	$(\lambda_3 / \lambda_1)^{½}$
Rusu (2009), Teo and Chie (2016)		$\lambda_3 / (\lambda_1 + \lambda_2 + \lambda_3)$	
Ordoñez et al (2017)		$\lambda_3 / (\lambda_1 \lambda_2)$ λ_2 / λ_3	$\lambda_3 \lambda_1 / \lambda_2^{\,2}$
Demantke et al (2011)	$(\lambda_1^{½} - \lambda_2^{½}) / \lambda_3^{½}$	$(\lambda_2^{½} - \lambda_3^{½}) / \lambda_1^{½}$	$(\lambda_3 / \lambda_1)^{½}$
Yokohama et al (2011) *a,b are adjustment coefficients	$\lambda_1 - a \lambda_2$	$\lambda_1 - \lambda_3$	$b \lambda_3$
Fukano and Masuda (2015)	λ_1 / λ_2	λ_1 / λ_2 λ_1 / λ_3	

Source: The authors (2023).

Table 3 – Further 3D features listed in the literature (Source: The authors).

Feature	Formula	Source
Anisotropy	$A= 1-\lambda_3 / \lambda_1$	Weinman et al. (2013)
Eigenentropy	$E=\lambda_1 \ln(\lambda_1)+\lambda_2 \ln(\lambda_2)+\lambda_3 \ln(\lambda_3)$	Weinman et al. (2013)
Ratio	λ_2 / λ_3	Fukano and Masuda (2015)

Source: The authors (2023).

2. Methodology

To derive spatial features from a point cloud, the principal components analysis is applied. Considering a set of 3D coordinates, the dispersion of the points around its centroid in the three-dimensional space (x1 x2 x3) is given by the variance-covariance matrix (C). The variance-covariance matrix is real, positive, semi-definite, and therefore its eigenvalues are always greater than or equal to zero. The eigenvalues are the scalars that satisfy equation 1.

$$det\ (C - \lambda I) = 0 \quad (1)$$

Eigenvalues and eigenvectors can be used to compute the principal components of the point cloud coordinates. Having computed the eigenvectors, the principal components transform can be applied, according to equation 2, to obtain the transformed point cloud.

$$Y = X * V \quad (2)$$

Where:
X (x_1 x_2 x_3) are the original coordinates
Y (y_1 y_2 y_3) are the transformed coordinates
V is a 3x3 matrix where each column stores an eigenvector.

The result is a new three-dimensional system, parallel to the main directions of the dispersion of the point cloud, as displayed in Figure 1, where three situations are illustrated: a) a case where there is no main direction in the point cloud dispersion; b) an elongated point cloud and c) a planar dispersion.

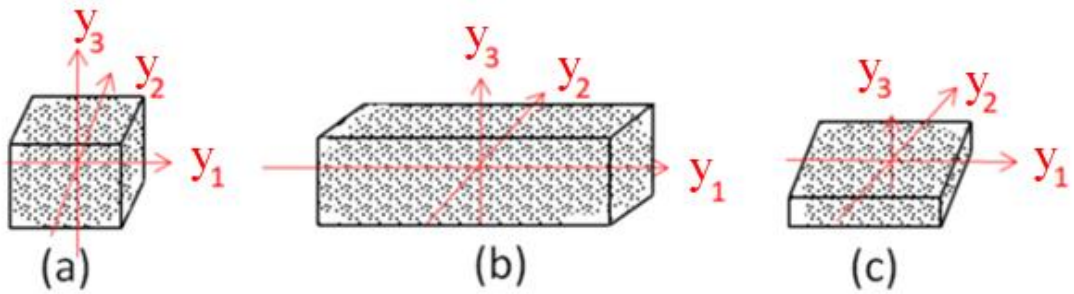

Figure 1 – The eigenvectors of different 3D shapes.
Source: The authors (2023).

From the principal components' theory, it is known that the main direction is oriented parallel to the eigenvector computed from the larger eigenvalue. The total variance in the original set is given by the sum of the variances in each axis and it is also equal to the sum of the eigenvalues. Alternatives for the description of the global variation of the coordinates can be achieved using the geometric mean (omnivariance).

As the amount of the total variance in the original set is given by the sum of the eigenvalues, the relative portion of the explained variance of each component is given by the ratio between the size of the associated eigenvalue and the total variance:

$$a_i = \lambda_i / (\lambda_1 + \lambda_2 + \lambda_3) \quad (3)$$

with $\lambda_1 > \lambda_2 > \lambda_3$

The normalized eigenvalues (a) can be used instead of the original eigenvalues, according to equation 3. This practice avoids scale problems (El-Halawany, 2013) and the analysis can focus on the shape. The sum of the normalized eigenvalues is always one, as displayed in equation 4. This is the equation of a plane in the three-dimensional space, as displayed in figure 2, a property that can be used to simplify the analysis.

$$a_1 + a_2 + a_3 = 1 \quad (4)$$

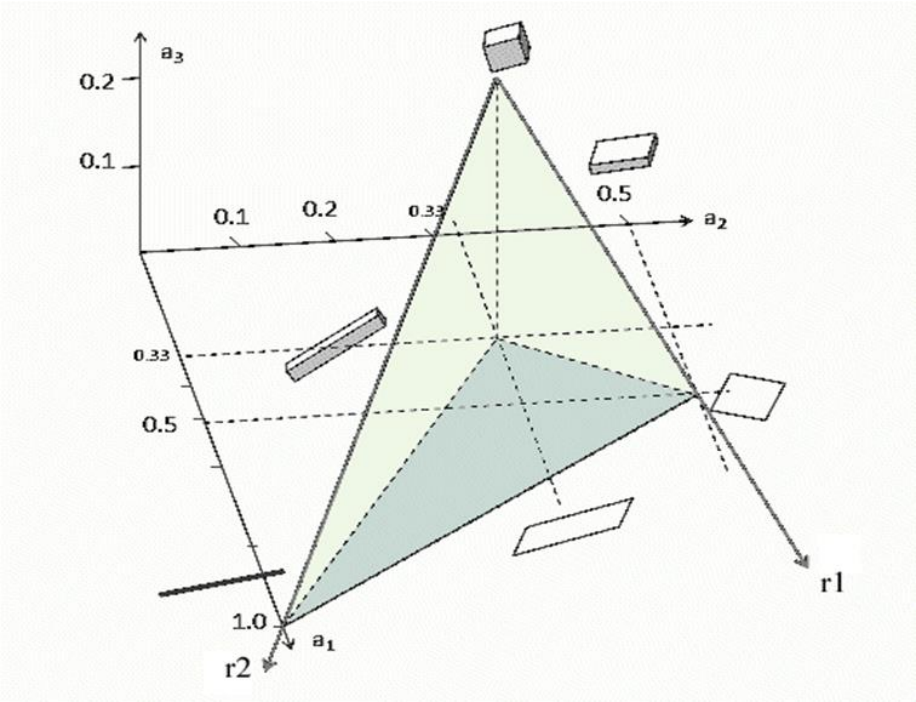

Figure 2 – Three-dimensional representation of the plane described in Equation 4.
Source: The authors (2023).

As there are some restrictions that derive from the definition of the eigenvalues ($1> a_1 > a_2 > a_3 > 0$) there is a limited region on this plane that the triplet (a_i, a_2, a_3) can occupy. For example, while a_1, can vary between 0 and 1, a_2 ranges between 0 and 1/2 because, by definition, it cannot be larger than a_1. In the same manner, a_3 ranges from zero to 1/3. As illustrated in figure 2, three extreme cases will be considered:

- Isotropic: In the extreme situation the eigenvalues are equal (1/3, 1/3, 1/3)
- Anisotropic, elongated: the shape is close to a line and the first eigenvalue is larger than the others. An ideal line would have null second and third eigenvalues (1,0,0)
- Anisotropic, planar: The third eigenvalue is relatively very small. The extreme case would be (1/2 1/2 0), a disk or a square. Depending on the relation of the first eigenvalues, the shape can also be elongated.

Considering the point (1/3, 1/3, 1/3) as the new origin, one can draw two lines (c1 and c2) that describe planarity or elongation. These lines are drawn in figure 2 as r1 and r2.

$$r_1: (a_1, a_2, a_3) = (⅓, ⅓, ⅓) + d\,(⅙, ⅙, -⅓) \quad (5)$$
$$r_2: (a_1, a_2, a_3) = (⅓, ⅓, ⅓) + e\,(⅔, -⅓, -⅓) \quad (6)$$

The plane where the triplets (a_1 , a_2, a_3) lie can be parametrized using the origin (1/3, 1/3, 1/3) and the two directional vectors r1 and r2, as displayed in equation 7. The location of the point on the plane, in relation to the origin following the directions r1 and r2 is given by the scalars "s" and "t" and is restricted by $s+t \leq 1$;

$$(a_1, a_2, a_3) = (⅓, ⅓, ⅓) + s\,⅙\,(1,1,-2) + t\,⅓\,(2, -1, -1) \quad (7)$$

Grouping terms results in equation 8.

$$(a_1-⅓ , a_2 -⅓ , a_3 -⅓) = s\,⅙\,(1,1,-2) + t\,⅓\,(2, -1, -1) \quad (8)$$

Equation 8 is composed by two basic operations: a shift and the sum of two vectors, being one 1/6(1 1 -2) responsible for describing the planarity and the second 1/3(2 -1 -1) describing the elongation. Making $b_i = a_i - 1/3$, we obtain three equations (Equations 9-11), where it can be proved that the third equation is a linear combination of the other two. This is not surprising, because a_3 can also be derived from a_1 and a_2, as $a_3 = 1 - a_1 - a_2$.

$$b_1 = \frac{1}{6} s + \frac{2}{3} t \quad (9)$$

$$b_2 = \frac{1}{6} s - \frac{1}{3} t \quad (10)$$

$$b_3 = -\frac{1}{3} s - \frac{1}{3} t \quad (11)$$

Then, the parameters can be computes solving equations 9 and 10. We call “s” planarity and “t” elongation. Both parameters vary between zero and one, but their sum cannot be greater than one.

$$s = 2 b_1 + 4 b_2 \quad (12)$$

$$t = b_1 - b_2 \quad (13)$$

or in terms of the normalized eigenvalues

$$s = 2 a_1 + 4 a_2 - 2 \quad (14)$$

$$t = a_1 - a_2 \quad (15)$$

Equations 14 and 15 allow describing the shape of a 3D point cloud using two easy to understand features. The first one related to the planarity of the cloud, when two dimensions are larger than the third one, and another related to elongated shapes. Both terms, planarity and elongation are easy to understand and therefore practical to describe shapes.

3. Results and discussion

To evaluate the efficiency of the proposed features, two experiments are presented. First, synthetic point clouds were produced with different shapes. These synthetic objects can be used to study and analyze the performance of the features. In the second experiment, real point cloud of objects attached to poles are analyzed. In the real situations, the point clouds do not cover the whole objects, as normally just one side is scanned during a mobile survey.

Test with artificial point clouds

To evaluate the validity of the proposed features, an artificial point cloud was produced with the equation of the sphere with radius equal to one. 1000 points were systematically computed on the sphere surface and then deformations parallel to the axis were introduced, as well as random noise varying from 0 to 1 in each axis. Finally, the point cloud was rotated in relation to the original axis. In Figure 3 the point cloud of an ellipse where the x dispersion along the axes has a proportion 4:3:1.

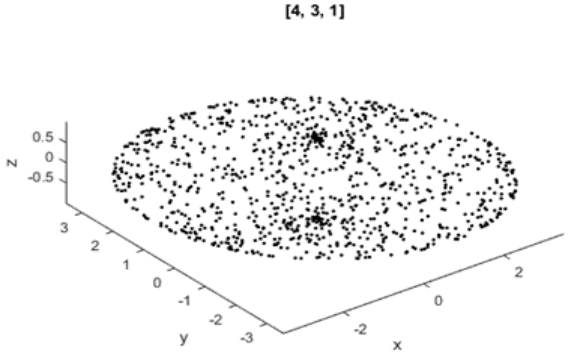

Figure 3 – Artificial point cloud describing the surface of an ellipsis.
Source: The authors (2023).

Varying the relative size of the dispersions, different ellipses were computed and classified as “planar" if s>0.5 and “elongated” if t>0.5. Some examples are listed in table 1, for illustration purposes. Those clouds that were not classified as planar or elongated are omitted.

Table 4 – Computed st-features for ellipses with varying proportion.

[proportion]	s	t	shape	[proportion]	s	t	shape
[1 0 0]	0.000	1.000	elongated	[4 1 1]	0.101	0.743	elongated
[1 1 0]	0.990	0.010	planar	[4 2 0]	0.395	0.605	elongated
[2 1 0]	0.395	0.605	elongated	[4 2 1]	0.183	0.551	elongated
[2 2 0]	0.990	0.010	planar	[4 3 0]	0.713	0.287	planar
[3 1 0]	0.197	0.803	elongated	[4 3 1]	0.517	0.266	planar
[3 1 1]	0.161	0.592	elongated	[4 3 2]	0.074	0.218	Not defined
[3 2 0]	0.609	0.391	planar	[5 4 2]	0.331	0.190	Not defined
[4 1 0]	0.116	0.884	elongated	[5 4 3]	0.067	0.128	Not defined

Source: The authors (2023).

Test with real 3d terrestrial scanner data

In this experiment, the objects located at the top of poles in an urban scene are classified. A terrestrial LiDAR survey in the campus of the Federal University of Paraná was used to obtain point clouds of real objects. The data used in this study was captured using the Pegasus One Mobile System and are described in Peixoto (2016). The system computes the trajectory based on the onboard GNSS and IMU and then enables computing a point cloud also with intensity information. The test area is located within the campus of the Federal University of Paraná, in the municipality of Curitiba, Brazil. The mobile scanner took two hours to survey 2.3 linear kilometers. The mean density of points for the study area was 2,400 points per m2 and were considered enough to detail the poles and shields.

First, the points on the ground were classified using the Classify Hard Surface method. The remainder points, associated to buildings, poles, cars and other objects were projected on a horizontal plane, using a grid as a basic structure. The grid size was established according to the relation between the spatial resolution of the point cloud and the expected diameter of the poles. The idea is that, if many points fall on a pole or another vertical structure, they will be projected on the same cell of the grid. So, the number of points on each cell was computed and stored as a grid value. In the next step, the grid values were separated according to the concentration of points (point density), enabling identification of vertical structures. The obtained regions were labelled using the connected components algorithm. In the next step, the pole is segmented according to the diameter variation and the top of the pole is obtained.

After the top is separated a reduced point cloud is available. It is assumed that the point set contains just points of the pole. Although, in some cases, the top may be mixed with other objects like vegetation. Figure 4 displays an example of the point cloud (in red) of a shield located at the top of a pole (black).

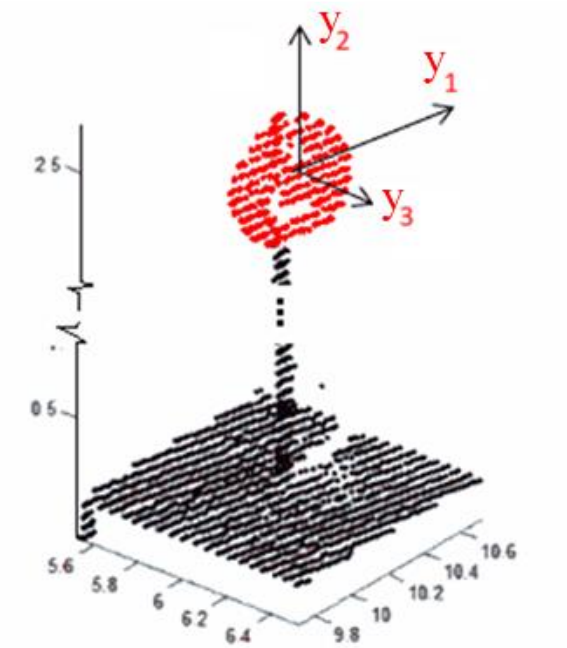

Figure 4 – Example of a segmented pole with one object attached to it (red) and the direction of the main eigenvectors.
Source: The authors (2023).

Five different objects were considered in the classification step. They are displayed in Figure 5. (e1) lamp with box; (e2) Lamp with four elements; (e3) Lamp with glass ball; (e4) Round shield; (e5) Square shield. The third class of lamps consists of a glass ball and therefore it is difficult to model from the point cloud, because of its transparency. The first class is a more complex structure because it is composed by two elements, a box, and a small horizontal lamp.

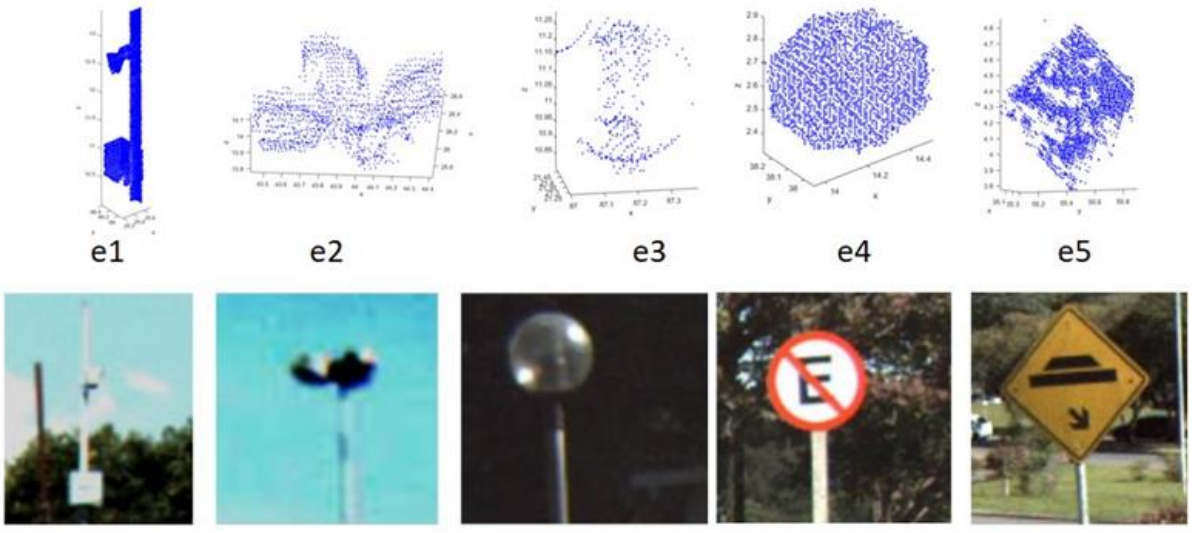

Figure 5 – Types of objects the top of the poles: (A) Lamp A; (B) Lamp with four elements; (C) Lamp with glass ball; (D) Round Shield; (E) Square Shield.
Source: Adapted from Peixoto (2016).

The normalized eigenvalues were computed for seven samples of each class. The resulting linearity and planarity features are plotted in figure 6 to illustrate the discussion.

The first class (e1) is composed of elongated objects, therefore the s-feature which describes them is very high and the t-factor almost null. On the other hand, classes e4 and e5 (round and square shields) present very different st-features, with high s-feature and low t-feature. Objects belonging to classes e2 and e3 are not planar, neither linear. This is visible in the st-space because they have st-features below 0.8. Nevertheless, they are not round enough to represent a significant volume. The lamps with a glass ball (class e3) could be described as round. But as the glass is transparent to the laser beam, fewer points are backscattered, and the shape is not characterized. The interior elements of the lamp are more visible giving this class an elongated shape. The lamp that is composed of four elements is flat and horizontal. Therefore, it is more planar, and this fact is visible in the plot, as the st-features values are close to the lower right corner.

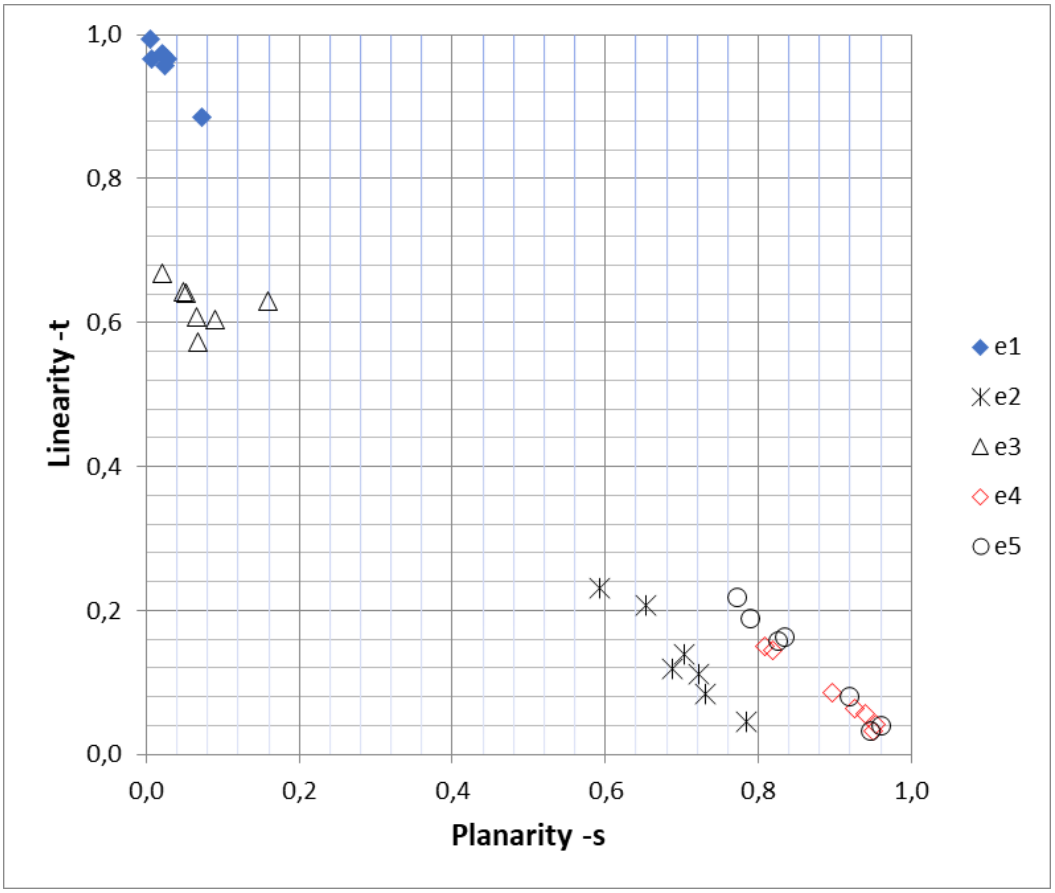

Figure 6 – Position of five different object groups in the st-feature space.

Source: The authors (2023).

The real shape of the objects is not reproduced in the point cloud because in some cases parts of the surfaces are not visible. This may occur because of occlusion as displayed in the e5 point cloud of figure 5; or in some cases only one side of the object is represented because of the scanning procedure. Nevertheless, the results reflect the differences between these objects.

It is worth to notice that the variation within the classes is parallel to the line that passes through (1,0) and (0,1). This means that for a given class, the sum of the features tends to be a constant, as shown in table 5. Extreme high mean values are visible for object classes with a more defined shape, elongated or planar (classes e1, e4 and e5). On the other hand, the sum of the features is smaller for the objects that are more 3D. Nevertheless, the standard deviation is still small. The

higher standard deviation of class e3 can be explained by the varying shape of the point clouds of this group. The variation is caused by the lack of reflected points and irregular distribution of the reflected points because of the glass ball.

The experiments with synthetic point clouds and real data allowed to verify the suitability to use the proposed "elongation' and "planarity" features to classify point clouds according to the shape. Both parameters do not consider the size of the cloud, as they are computed from the normalized eigenvalues. To complete the description, the sum of the eigenvalues can be included.

Table 5 – Mean and standard deviation of the sum of the st-features.

class	Mean(s+t)	Std(s+t)
e1	0.984	0.015
e2	0.830	0.018
e3	0.696	0.045
e4	0.981	0.015
e5	0.999	0.009

Source: The authors (2023).

Comparing the proposed features "elongation" and "planarity" with those listed in the literature and shown in table 2, some similarities can be found. The planarity feature "s" is the weighted sum of the first and second eigenvalues, giving double weight to the second one. As the sum of the normalized eigenvalues equals one, this feature indirectly compares the first two eigenvalues to the third one and resembles the equations proposed in the literature, like Rusu (2009), Teo and Chie (2016) and Ordoñez et al (2017). The linearity feature "t" is the difference between the first and second normalized eigenvalues, which is also present in the formulations used by Weinman et al. (2013), Demantke et al. (2011) or Yokohama et al (2011). The advantage that the "s" and "t" features are scale invariant and vary between zero and one.

The option to use two features and the understanding of their domain allows reducing the input vector size in the classification process. For example, Özdemir et al. (2019) use at least 11 spatial features, plus de height, computed from airborne LiDAR, to feed Recurrent Neural Networks and Convolutional Networks to classify two public datasets (Vaihingen and Dortmund). The use of 11 features includes redundancy that needs to be suppressed in the first layers of the net. Reducing the selected features would speed up the classification.

4. Conclusions

In this paper, two features are introduced to describe the shape of 3D objects scanned by a terrestrial mobile LiDAR. The pair of features describes planarity and elongation and is coherent with those described in the literature. It was shown that, by normalizing the eigenvalues, the effect of the size of the objects can be eliminated and the features can better describe the shape. It is also shown that two features are enough to describe shape and that these features are simple linear combinations of the eigenvalues. The advantage of the proposed features is that they allow choosing thresholds, as they are normalized in the range between zero and one. This allows easier description of the shape in terms of just two well-known terms. The proposed method enables accurate description of the object surface by two parameters related to planarity and elongation. The combination of these parameters enables classifying point clouds into linear, planar, and spherical objects. The results of tests with simulated and real objects validated the proposal and show that the derived features can be used to classify pole tops from a terrestrial LiDAR survey. The results are strongly affected by the point density in relation to the size of the object and occlusion. As expected, better results were achieved when the objects were closer to the measuring device.

Acknowledgments

The authors would like to thank ESTEIO Engenharia e Levantamentos S.A for allowing the use of the data and CAPES and CNPq (process nr.: 307086/2021) for the support.

References

ALONSO, I.; Riazuelo, L.; Montesano, L.; Murillo, A.C. 3D-MiniNet: Learning a 2D Representation from Point Clouds for Fast and Efficient 3D LIDAR Semantic Segmentation. *IEEE Robot. Autom. Lett*., 5, pp. 5432–5439, 2020.

BOLLES, R. C.; Fischler, M. A. A RANSAC-based approach to model fitting and its application to finding cylinders in range data. *In Int. Joint Conf. on Art. Intelligence*, Vancouver, Canada, pp. 637–643, 1981.

DENIS, E.; Burck, R.; Baillard, C. Towards road modeling from terrestrial laser points, *The International Archives of the Photogrammetry*, Vol. XXXVIII, Part 3A, pp.293-298, 2010.

DEMANTKE, J.; Mallet, C.; David, N.; Vallet, B. Dimensionality based scale selection in 3D LiDAR point clouds. *ISPRS Workshop on Laser Scanning 2011*, Calgary, Canada, 29–31 August, 6p (on CDROM), 2011.

DIAZ-VILARINO, L.; Conde, B.; Lagüela, S.; Lorenzo, H., Automatic Detection and Segmentation of Columns in As-Built Buildings from Point Clouds. *Remote Sensing*, 7(11), pp.15651-15667, 2015.

EL-HALAWANY, S. *Detection of Road Furniture from Mobile Terrestrial Laser Scanning Point Clouds*, Ph.D. thesis, Department of Geomatics Engineering, University of Calgary, Canada, 2013.

FALTÝNOVÁ, M.; Matoušková, E.; Šedina, J. ; Pavelka, K. Building facade documentation using laser scanning and photogrammetry and data implementation into BIM. *The International Archives of the Photogrammetry, Remote Sensing and Spatial Information Sciences*, Volume XLI-B3, 2016. XXIII ISPRS Congress, 12–19 July 2016, Prague, Czech Republic, 2016.

FERNANDES, D.; Silva, A.; Névoa, R.; Simões, C.; Gonzalez, D.; Guevara, M.; Novais, P.; Melo-Pinto, P. Point-cloud based 3D object detection and classification methods for self-driving applications: A survey and taxonomy. *Information Fusion*, 68, pp. 161-191, 2021.

FUKANO, K.; Masuda, H. Detection and classification of pole-like objects from mobile mapping data. *ISPRS Annals of Photogrammetry, Remote Sensing and Spatial Information Sciences*, 1, pp. 57-64, 2015.

GUAM, H.; Yu, Y.; Ji, Z.; Li, J. Zhang, Q. Deep learning-based tree classification using mobile LiDAR data, *Remote Sensing Letters*, 6:11, pp.864-873, 2015.

GUAM, H.; Yan, W.; Yu, Y.; Zhong, L.; Li, D. Robust traffic-sign detection and classification using mobile lidar data with digital images. *IEEE journal of selected topics in applied earth observations and remote sensing*, vol. 11, no. 5, 2018.

HAGHIGHATGOU, N.; Daniel, S.; Badard, T. A method for automatic identification of openings in buildings facades based on mobile LiDAR point clouds for assessing impacts of floodings, *International Journal of Applied Earth Observation and Geoinformation*, Volume 108, 2022.

HRUTKA, B.P.; Z. Siki, Z.; Takács, B. Voxel-based point cloud segmentation and building detection. *The International Archives of the Photogrammetry, Remote Sensing and Spatial Information Sciences*, Volume XLVIII-4/W1-2022. Free and Open Source Software for Geospatial (FOSS4G) 2022 – Academic Track, Florence, Italy, 22–28 August 2022.

HUANG, J.; You, S. Pole-like object detection and classification from urban point clouds. *IEEE International Conference on Robotics and Automation (ICRA)*, pp. 1-7, 2005.

HUANG, J.; You, S. Point Cloud Labeling using 3D Convolutional Neural Network. 23rd *International Conference on Pattern Recognition (ICPR),* Cancún Center, Cancún, México, December 4-8, 2016.

IBRAHIM, S.; Lichti, D. Curb-based street floor extraction from mobile terrestrial LiDAR point cloud. *International Archives of the Photogrammetry, Remote Sensing and Spatial Information Sciences*, Volume XXXIX-B5, 2012. XXII ISPRS Congress, Melbourne, Australia, 25 August – 01 September 2012.

LI, F.; Elberink, S. O.; Vosselman, G. Pole-like street furniture decomposition in mobile laser scanning data. *ISPRS Annals of the Photogrammetry, Remote Sensing and Spatial Information Sciences*, Volume III-3, 2016. XXIII ISPRS Congress, Prague, Czech Republic, 12–19 July 2016.

LI, J.; Cheng, X. Supervoxel-based extraction and classification of pole-like objects from MLS point cloud data. *Optics & Laser Technology*, Volume 146, February, 2020.

LI, Y.; Wang, W.; Li, X.; Xie, L.; Wang, Y.; Guo, R.; Xiu, W.; Tang, S. Pole-Like Street Furniture Segmentation and Classification in Mobile LiDAR Data by Integrating Multiple Shape-Descriptor Constraints. *Remote Sensing* 11(24), 2019.

LUO D.; Wang Y. Rapid extracting pillars by slicing point clouds, *International Archives of the Photogrammetry Remote Sensing*, vol.36-8, pp.71-75, 2008.

ORDONES, C.; Cabo, C.; Sanz-Ablanedo, E. Automatic detection and classification of pole-like objects for urban cartography using mobile LASER scanning data. *Sensors*, 17, 1465; pp 1-10, 2017.

ÖZDEMIR, E.; Remondino, F.; Golkar, A. Aerial point cloud classification with deep learning and machine learning algorithms. *The International Archives of the Photogrammetry, Remote Sensing and Spatial Information Sciences*, Volume XLII-4/W18, 2019 GeoSpatial Conference 2019 – Joint Conferences of SMPR and GI Research, Karaj, Iran, 12–14 October 2019.

PEIXOTO, E.B.A., *Detecção e identificação automática de postes utilizando nuvem de pontos do sistema laser terrestre móvel*. Dissertação de mestrado no Programa de Pós-Graduação em Ciências Geodésicas da Universidade Federal Do Paraná, pp. 109-110, 2016.

PRESS P.; Austin, D. Approaches to pole detection using ranged laser data. *Proceedings of Australasian Conference on Robotics and Automation*, Citeseer. pp.1–8, 2004.

QI, C.R.; Su, H.; Mo, K.; Guibas, L.J. PointNet: deep learning on point sets for 3D classification and segmentation. *Proceedings of the IEEE Conference on Computer Vision and Pattern Recognition* (CVPR), pp. 652-660, 2017.

QI, C.R., Yi, L. K.; Su, H.; Guibas, L.J. Pointnet++: Deep hierarchical feature learning on point sets in a metric space, *Adv. Neur. Inform. Process. Syst*. Pp. 5099–5108, 2017.

REED, I.S.; Yu, X. Adaptive multiple-band CFAR detection of an optical pattern with unknown spectral distribution. *IEEE Trans. Acoust. Speech Signal Process.* 1990, 38, 1760–1770, 1990.

RODRÍGUEZ-CUENCA, B., García-Cortés, S., Ordóñez, C., Alonso, M. C. Automatic detection and classification of pole-like objects in urban point cloud data using an anomaly detection algorithm. *Remote Sensing* 2015, 7, 12680-12703, 2015.

RUSU, R. B. *Semantic 3D object maps for everyday manipulation in human living environmen*ts. PhD thesis, Computer Science department, Technische Universitat Munchen, Germany, 2009.

SHI, Z.; Kang, Z.; Lin, Y.; Liu, Y.; Chen, W. Automatic Recognition of Pole-Like Objects from Mobile Laser Scanning Point Clouds. *Remote Sensing* 2018, 10(12), p.1891, 2018.

SIRMACEK, B.; Lindenbergh R. Automatic classification of trees from laser scanning point clouds. SPRS Annals of the Photogrammetry, Remote *Sensing and Spatial Information Sciences*, Volume II-3/W5, 2015. ISPRS Geospatial Week 2015, La Grande Motte, France, 28 Sep – 03 Oct 2015.

SUWARDHI, D.; Fauzan, K.N.; Harto, A.B.; Soeksmantono, B.; Virtriana, R.; Murtiyoso, A. 3D Modeling of Individual Trees from LiDAR and Photogrammetric Point Clouds by Explicit Parametric Representations for Green Open Space (GOS) Management. *ISPRS Int. J. Geo-Inf.* 2022, 11(3), 174, 2022.

SU, H.; Maji, S.; Kalogerakis, E.; Learned-Miller, E., Multi-view Convolutional Neural Networks for 3D Shape Recognition. In Proceedings of the 2015 IEEE International Conference on Computer Vision (ICCV), Santiago, Chile, 7–13 December 2015; pp. 945–953.2015.

TEO, T.-A.; Chiu, C.-M. Pole-like road object detection from mobile Lidar system using a coarse-to-fine approach. IEEE Journal of selected topics in applied earth observations and remote sensing, vol. 8, no. 10, 2015.

WEINMANN, M.; Jutzi, B.; Mallet, C. Feature relevance assessment for the semantic interpretation of 3d point cloud data. *ISPRS Annals of the Photogrammetry, Remote Sensing and Spatial Information Sciences*, Volume II-5/W2, 2013 ISPRS Workshop Laser Scanning 2013, Antalya, Turkey, 11 – 13 November 2013.

YAN, W. Y.; S. Morsy, A. Shaker, and M. Tulloch. Automatic Extraction of Highway Light Poles and Towers from Mobile LiDAR Data. *Optics & Laser Technology*, Vol. 77, pp. 162–168, 2016.

YANG, B., Dong, Z., 2013. A shape-based segmentation method for mobile laser scanning point clouds. ISPRS Journal of Photogrammetry and Remote Sensing 81 pp. 19–30, 2013.

YOKOYAMA, H.; Date, H.; Kanai, S.; Takeda, H. Pole-like objects recognition from mobile laser scanning data using smoothing and principal component analysis. *International Archives of the Photogrammetry, Remote Sensing and Spatial Information Sciences*, Volume XXXVIII-5/W12, 2011. ISPRS Calgary 2011 Workshop, 29-31 August 2011.

YOKOYAMA, H.; Date, H.; Kanai, S.; Takeda, H. Detection and classification of pole-like objects from mobile laser scanning data of urban environments. *International Journal of CAD/CAM* Vol. 13, No. 2, pp. 31–40, 2013.

YU, Y., Li, J., Guan, H., Wang, C., Yu, J. Semiautomated extraction of street light poles from mobile lidar point-clouds. *IEEE transactions on geoscience and remote sensing*, vol. 53, no. 3, 2015.